26th INTERNATIONAL CONGRESS ON SOUND AND VIBRATION
7-11 July 2019, Montreal

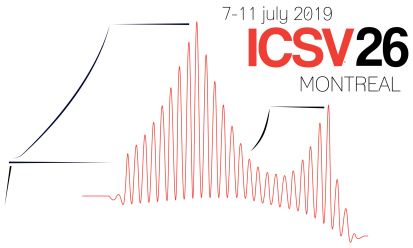

ANALYTICAL PREDICTION OF BOUNDARY LAYER INGESTION NOISE FOR AN INTEGRATED TURBOFAN

Martin Staggat, Antoine Moreau and Sébastien Guérin
German Aerospace Center (DLR), Institute of Propulsion Technology, Berlin, Germany
email: martin.staggat@dlr.de, antoine.moreau@dlr.de, sebastien.guerin@dlr.de

A parametric study based on the analytical predictions of tonal and broadband noise for a generic turbulent boundary layer interacting with the rotor of an ultra high bypass ratio fan is presented. The approach and take-off conditions are considered. To classify the importance of ingestion noise, the rotor-stator interaction noise of the fan stage is also evaluated analytically based on computational fluid dynamic simulations. The implemented analytical boundary layer model provides the axial mean velocity profile and also the axial and transversal turbulent quantities. This allows to consider the turbulence within the boundary layer as anisotropic. The acoustic response of the rotor blades is predicted by using a modified theory for the acoustic radiation from an airfoil. The predicted tonal sound power levels are similar for the ingestion noise and the rotor-stator wake interaction noise at take-off conditions. For approach conditions the tonal boundary layer interaction noise is dominated by the rotor-stator wake interaction noise. The influence of the boundary layer thickness and the a shape factor, linked to the axial pressure gradient, on tonal noise is discussed. Concerning broadband noise the results indicate that the boundary layer interaction noise has the potential to dominate the low to mid frequency range compared to rotor-stator interaction noise. The predicted power spectral density levels show that the ingestion noise increases with boundary layer thickness and shape factor.

Keywords: engine acoustics, boundary layer ingestion

1. Introduction

The present-day improvements concerning the fuel efficiency of civil aircraft are mainly driven by a continuous increase of the engines bypass ratio and therefore accompanied by an increase of the engine diameter. In the mid to long term this trend may lead to a transformation of the classical tube-wing aircraft architecture towards configurations with highly integrated or even embedded engines benefiting from boundary layer ingestion (BLI), such as blended or hybrid wing bodies [1]. Beside potential advantages in terms of an increased propulsion efficiency, concerns arise about new noise sources caused by the highly distorted flow interacting with the fan blades.

The DLR in-house analytical engine noise prediction tool PROPNOISE allows the investigation of several tonal and broadband noise (BBN) sources [2]. In two earlier publications [3, 4] a theory for the prediction of BBN, caused by the interaction of a rotor with a turbulent boundary layer, was developed and improved. In these past studies, the theory used was flow-informed, based on hot-wire measurement data providing the mean and turbulent mean velocities for an open rotor benchmark. For the present study

an analytical turbulent boundary layer model was implemented. This model provides the aerodynamic excitation data for the acoustic models based on a few parameter, such as the boundary layer thickness or the free-stream velocity, without the need of measurement data.

The paper is organized as follows: Section 2 outlines the analytical boundary layer model and the applied modified acoustic theory. Section 3 applies the theory on an up-scaled version of DLR's ultra high bypass ratio (UHBR) engine [5] ingesting a generic boundary layer. A parametric study, which is varying the boundary layer thickness δ_{99} and the shape factor H_{12}, linked to the pressure gradient in mean flow direction, is performed. The tonal and broadband BLI noise predictions are compared with rotor-stator wake interaction (RSI) noise predictions informed by computational fluid dynamics (CFD). Finally Section 4 summarizes the findings of this study.

2. Modeling of aerodynamic excitation and acoustic radiation

The theory contains the modeling of the aerodynamic excitation caused by the turbulent boundary layer and the generated acoustic radiation of the rotor blades.

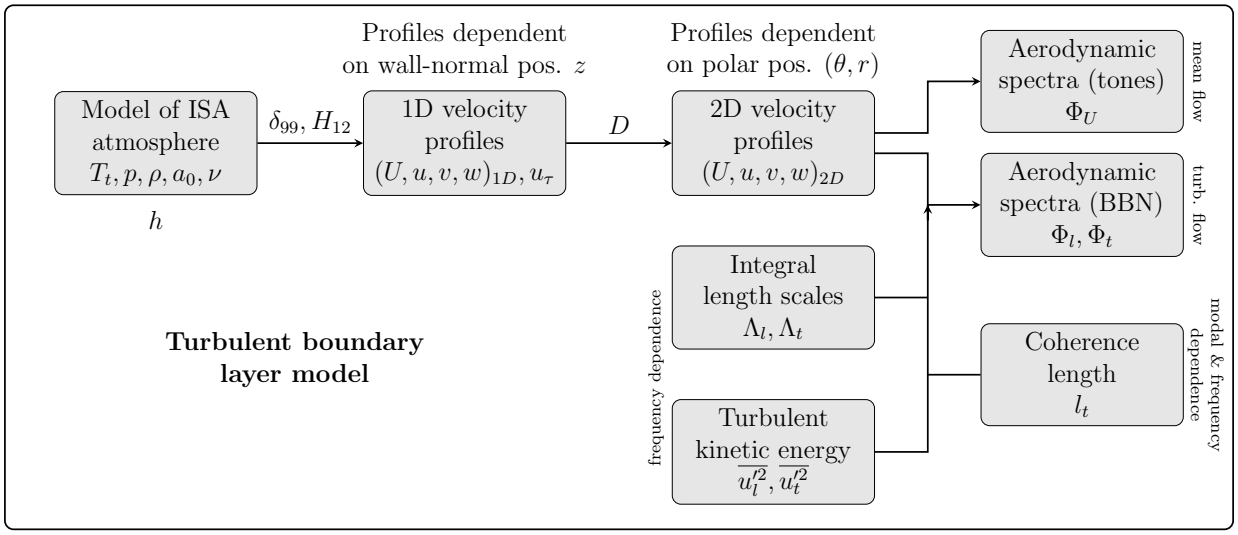

Figure 1: Components constituting the implemented turbulent boundary layer model.

Figure 1 represents the components constituting the boundary layer model. It is assumed that the boundary layer is caused by a flat plate. In a first step, the local properties of the international standard atmosphere (ISA), such as the total temperature T, the static pressure p, the density of air ρ, the speed of sound a_0 and the kinematic viscosity ν, are defined based on the flight altitude h. The friction velocity u_τ is determined based on the boundary layer thickness δ_{99} and the free-stream velocity U_∞ assuming a logarithmic velocity profile. By following Cole's [6] suggestion for a turbulent shear flow, the final mean velocity profile U is computed based on the shape factor H_{12}. This parameter is the ratio of the displacement to the momentum loss thickness and therefore highly dependent on the pressure gradient in mean flow direction. The turbulent mean velocities u, v and w are computed based on Prandtl's mixing length hypothesis extended by the modifications of van Driest and Escudier to account for the conditions in a boundary layer shear flow [7]. The hereby estimated velocity profiles are assumed to continue equally parallel to the flat plate. With reaching the boundary layer thickness δ_{99} normal to the flat plate, a uniform mean flow velocity of U_∞ and a vanishing of the turbulent mean velocities is assumed. Based on the rotor diameter D and the wall-normal position of the engine axis the region of the 2D-velocity-profiles, ingested into the engine, is transformed on polar coordinates. For the excitation of the tonal BLI

noise, the mean velocity profile is decomposed into circumferential aerodynamic modes of order m_0 at every radial position and the excitation frequencies are known a priori at the blade passing frequency (BPF) and its higher harmonics. For the BBN source, the frequency dependence is modelled by one-dimensional anisotropic turbulence spectra based on Kerschen and Gliebe [4, 8]. Therefore a modeling of the turbulent longitudinal and transversal integral length scale Λ_l and Λ_t is necessary. The modeling of the integral length scales is based on the streamwise length scale Λ_s according to Hunt and Morrison [9]. The distribution of turbulent kinetic energy (TKE) across the aerodynamic modes is achieved by the use of a Gaussian distribution function as shown in Staggat et al. [3, 4]. By using an analytically modelled circumferential coherence length according to Haxter and Spehr [10], this function ensures an energy distribution dependent on the circumferential extend of an ingested coherent boundary layer structure and is therefore an important aspect in the modeling of the turbulence anisotropy. Finally, Fig. 2 illustrates the shapes of the mean and turbulent velocity profiles dependent on δ_{99} and H_{12} for the investigated parameter sets at approach (AP) conditions. In addition the radially averaged longitudinal integral length scale is given normalized on its value Λ_l^* for $\delta_{99} = 0.15 \cdot D$ and $H_{12} = 1.35$ as a legend box in Fig.2 (right). Note, that in the present study Λ_t is assumed to be proportional to Λ_l by a factor.

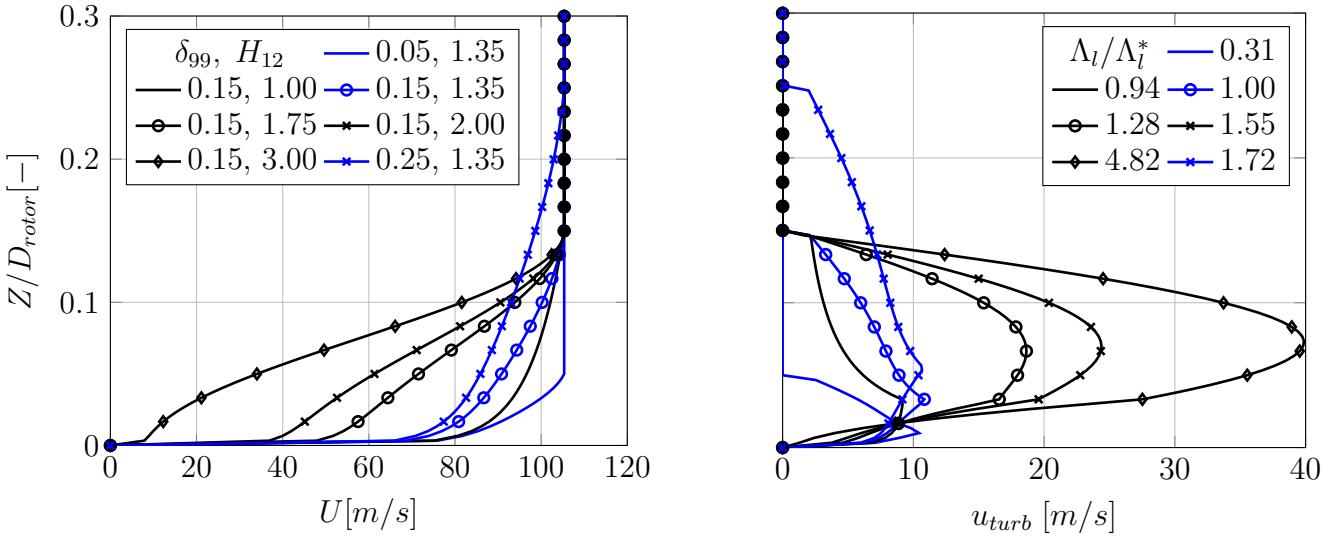

Figure 2: Parameter variation of the boundary layer thickness δ_{99} and shape factor H_{12} for AP. Left: mean velocity profiles, right: summation of turbulent mean velocity profiles $u_{turb}^2 = \overline{u'^2} + \overline{v'^2} + \overline{w'^2}$.

Model of acoustic radiation

The in-duct solution for the tonal and broadband pressure is formulated in form of modal amplitudes according to Moreau [2]. For BBN the expectation value of the squared absolute value of the modal amplitudes is based on Moreau [2] extended by the modification described in Staggat et al. [3, 4] to account for correlated rotor blades.

According to Fig.3 for BBN the modal amplitudes for uncorrelated rotor blades are subject to a modification by a modal weighting function $\Sigma(m)$. This function models the correlation of consecutive rotor blades, resulting from the ingestion of axially stretched coherent structures, constituting the assumed anisotropy within the turbulent boundary layer. The estimation of the correlation length, over which consecutive rotor blades

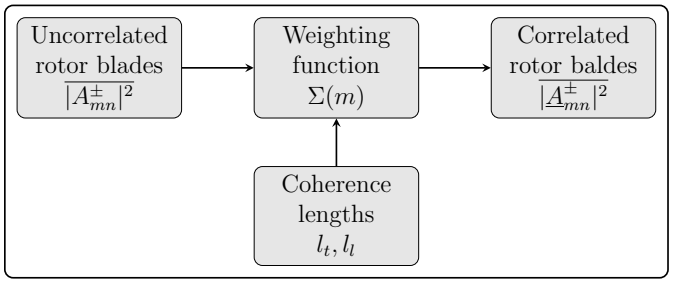

Figure 3: Modeling of correlated rotor blades for broadband noise.

are correlated with each other, is based on a longitudinal coherence length modelled according to Haxter and Spehr [10] and the rotational speed of the rotor. In case of correlated rotor blades this weighting function predicts the preferred excitation of distinct interaction modes, resulting in peaks in the BBN spectrum, centered at the BPF and its higher harmonics. Note that in general $l_t \ll l_l$ holds for the coherence lengths [2, 3, 4].

3. Application

The investigated fan is an up-scaled version of DLRs UHRB fan [5]. Key operating parameters, such as the fan pressure ratio (FPR) and the relative axial Mach number $M_{\text{x,rel}}$, are given in Tab. 1. The relative Mach number $M_{\text{tip, rel}}$ does not exceed one until the tip for End of Field (EoF). Thus a comparison with RSI instead of shock or buzz-saw noise is justified.

Table 1: Key parameters of investigated OPs and design (DP) of DLR's up-scaled UHBR fan [5].

	AP	EoF	DP
FPR	1.09	1.29	1.31
$M_{\text{tip, rel}}$	0.59	1.00	1.04
$M_{\text{x, rel}}$	0.31	0.55	0.58

Figure 4 illustrates the complete PROPNOISE work-flow: for the standalone mode, used for the prediction of the BLI noise, basic engine geometric parameters, such as the hub- and tip-diameters, axial segment lengths and the rotor blade and stator vane count, have to be specified. In addition, the design operating point (DP) is defined by its mass flow and the according rotational speed of the rotor. Based on these key parameters, a re-staggering of the rotor and stator stagger angles is performed. As a result, the specified DP is coinciding with the fan stages maximum of isentropic efficiency. Herewith, the rotor and stator geometry is fully defined and the aerodynamic excitation of BLI noise at AP and EoF can be computed. The rotor-stator wake interaction noise is computed based on 3D RANS flow solutions for AP and EoF. The mean and turbulent flow quantities as well as geometrical parameters, such as leading and trailing edge positions, are extracted and used to reconstruct the aerodynamic excitation of RSI noise [2, 11]. Note that the turbulent boundary layer model of Section 2 and the 3D RANS flow data provide the radially resolved aerodynamic excitation.

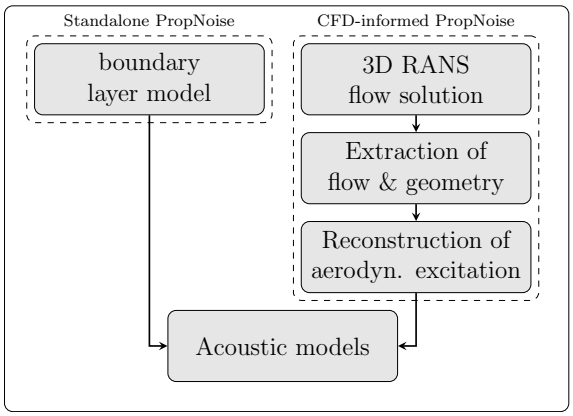

Figure 4: Overview of PROPNOISE work flow of the used stand-alone and CFD-informed modes.

3.1 Tonal results

Figure 5 shows result for the sound power level (PWL) at 1st to 5th BPF for BLI and RSI noise. Note that the RSI noise source is assumed to be unaffected by the presence of the boundary layer in the present study. Due to the cut-off design of the fan stage no RSI noise is predicted for the 1st BPF at AP. However, a comparison of the overall sound power level (OAPWL) reveals that RSI noise (139 dB) is still dominating the BLI noise (117 dB). For EoF the difference in OAPWL is less distinct (145 dB for BLI and 148 dB

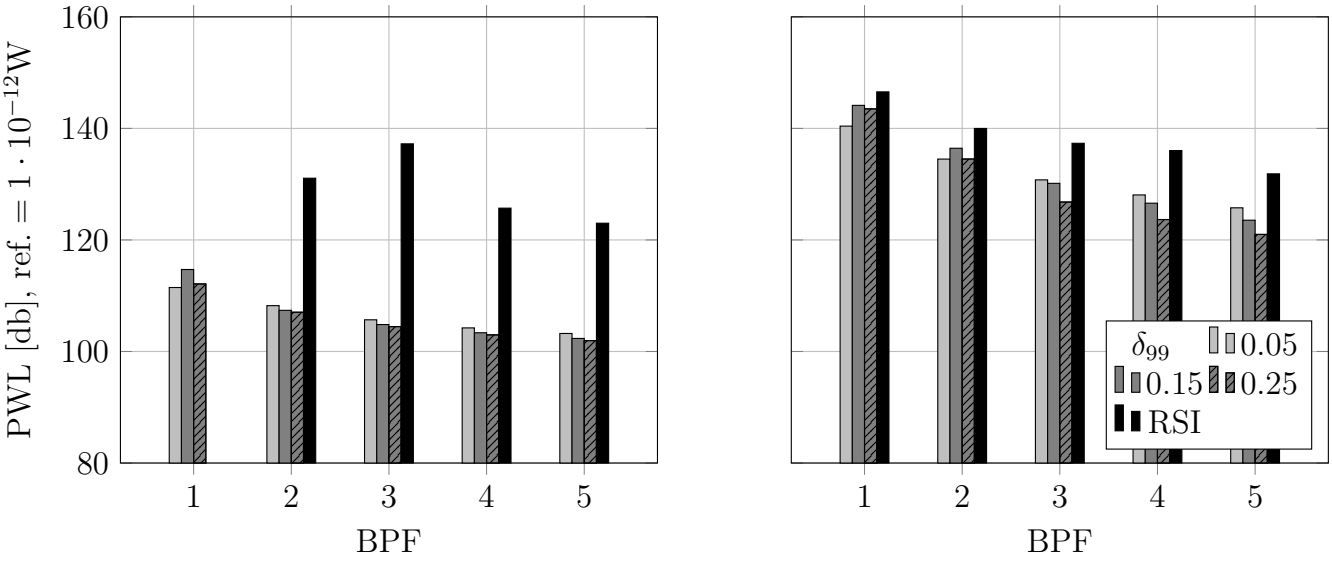

Figure 5: PWL of tonal noise sources for Approach (left) and End of Field (right) for different boundary layer thicknesses δ_{99} at near zero pressure gradient ($H_{12} = 1.35$).

for RSI). For AP aerodynamic modes $m_0 \in [13, 31]$ excite cut-on acoustic modes $m \in [-9, 9]$ at 1st BPF. For EoF this band is increased to $m_0 \in [41, 3]$ and $m \in [-19, 19]$ for the 1st BPF. Since the boundary layer excites all acoustic modes an increase of cut-on modes, excited by strong low aerodynamic mode orders, generally yields a significant increase of PWL with increasing rotational speed from AP to EoF. An increase of the boundary layer thickness is accompanied by a PWL reduction for the 2nd to 5th BPF for AP and for the 3rd to 5th BPF for EoF. For the remaining frequencies the increase of δ_{99} initially increases the PWL ($\delta_{99} = 0.15\,\mathrm{D}$) before a reduction of PWL is observed again for $\delta_{99} = 0.25\,\mathrm{D}$. This trend can be explained by the aerodynamic excitation: the increase of boundary layer thickness non-simple alters the amplitudes of the lower aerodynamic mode orders $m_0 < 25$ that are dominating the excitation of 1st BPF at AP and 1st to 2nd BPF at EoF. In contrast the amplitudes of aerodynamic mode orders $m_0 > 25$, dominating the excitation of the higher BPFs, are slightly reduced with an increase of δ_{99}.

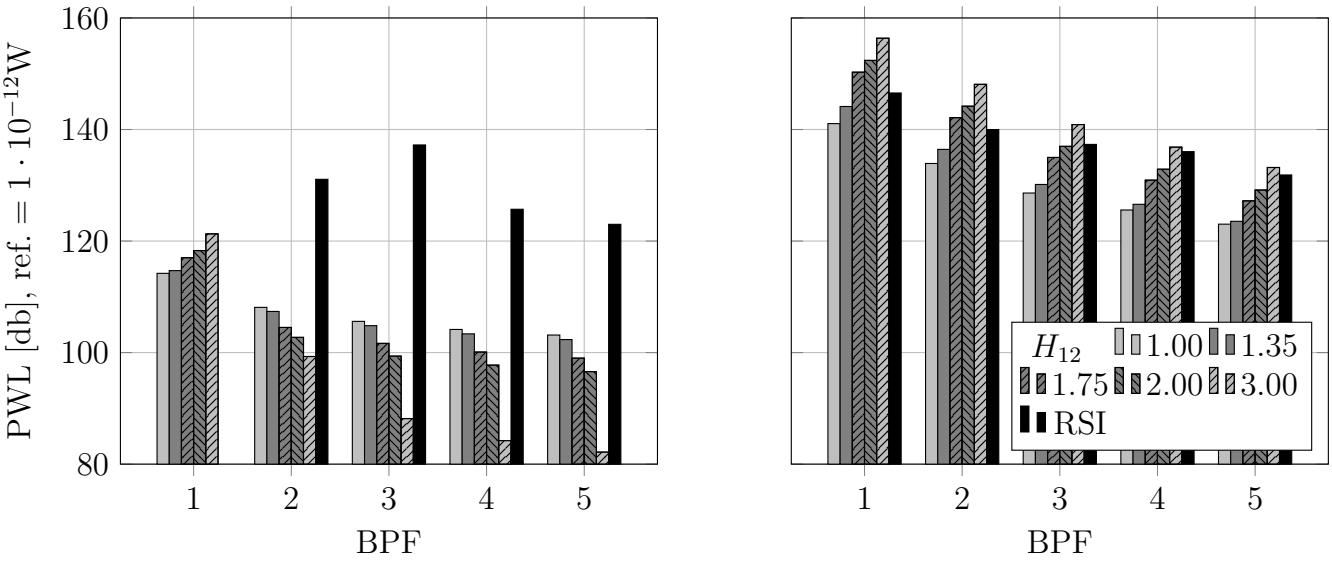

Figure 6: PWL of tonal noise sources for Approach (left) and End of Field (right) for different shape factors H_{12} at $\delta_{99} = 0.15\,\mathrm{D}$.

Figure 6 compares PWL predictions for different shape factors. For $H_{12} \lesssim 1.3$ the flow is accelerated by a negative pressure gradient, whereas $H_{12} \gtrsim 1.3$ indicates a positive gradient, decreasing the boundary layer stability. Finally at $H_{12} = 4.0$ a detachment of the boundary layer flow at the wall will occur. For AP the increase of H_{12} leads to an increased PWL for the 1st BPF of the BLI noise. For the 2nd to 5th BPF the increase is accompanied by an decreased PWL. In contrast the results at EoF show a continuous increase of BLI noise with increasing H_{12}. Whereas RSI remains the dominant source for AP, the BLI noise has the potential to dominate RSI for a sufficient hight shape factor ($H_{12} \geq 1.75$) at EoF.

The contrary trends of the change of PWL with H_{12} for AP and EoF are caused by an excitation and propagation effect: The increase of H_{12} leads to an increase of the amplitudes of lower aerodynamic mode orders $m_0 < 30$. Amplitudes of aerodynamic modes $m_0 > 30$ are decreased with increasing H_{12}. For AP the 1st BPF is purely excited by aerodynamic modes of order $m_0 < 30$. The excitation of the 2nd to 5th BPF is achieved by aerodynamic modes of higher order $m_0 > 30$ whose amplitudes decrease with increasing H_{12}. For EoF the region of aerodynamic modes $m_0 < 30$ is always dominantly involved in the excitation of all BPFs. Therefore the observed trend is opposite for the 2nd to 5th BPF compared to AP.

3.2 Broadband results

Figure 7 shows results for the power spectral density of sound power (PSD) at AP and EoF for different boundary layer thicknesses. In addition the 1st to 3rd BPFs are tagged by vertical lines for both operating points. A comparison of both operating points reveals an in general higher PSD for EoF. In addition the spectrum is shifted towards higher frequencies due to the increased rotational speed of the rotor. For EoF peaks at the BPF and its higher harmonics are clearly visible in the BLI noise spectra. Those result from the modelled correlation of consecutive rotor blades chopping the same axially-stretched coherent structures. For AP the rotational speed is to low and this correlation is nearly lost. In both cases an increase of δ_{99} leads to an increased PSD since the region containing turbulence, and therefore the total amount of TKE, is increased (see profiles for $H_{12} = 1.35$ in Fig. 2, right). It can be seen that in the present study the BLI noise source has the potential to dominate the RSI source in the low and mid frequency range.

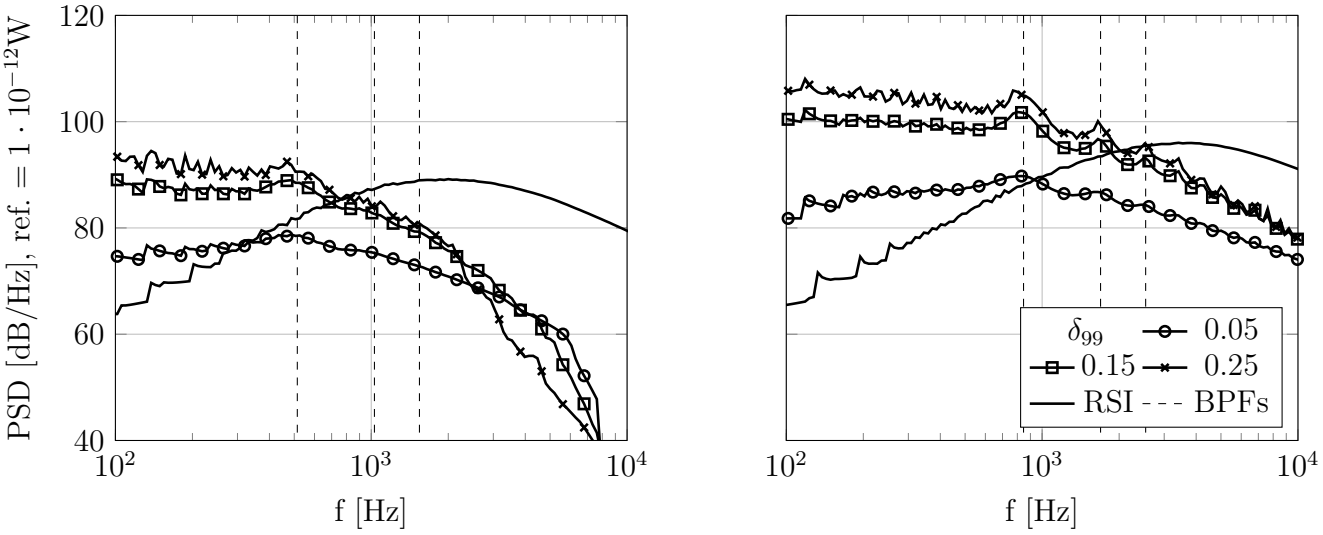

Figure 7: PSD of broadband noise source for Approach (left) and End of Field (right) for different boundary layer thicknesses δ_{99} at neutral pressure gradient ($H_{12} = 1.35$).

For AP the OAPWL for BLI of $122\,\mathrm{dB}$ is dominated by RSI with $126\,\mathrm{dB}$. This trend is changed for

EoF (OAPWL of $136\,\mathrm{dB}$ for BLI and $134\,\mathrm{dB}$ for RSI). Note that this conclusion is strongly dependent on the modelled integral length scales. Lower scales will shift the spectral peak from the left upper quadrant towards the right lower quadrant, similar to RSI.

The last parametric study compares the PSD at AP and EoF for different shape factors H_{12}. Again, the PSD for AP is in general lower and more shifted to the low-frequency domain due to the lower rotational speed. Peaks, centered at the BPF harmonics occur for all shape factors at EoF. For AP and EoF an increase of H_{12} is accompanied with an increase of the predicted PSD. The reason for this increase is the proportionality of the used algebraic turbulence model to the gradient of the mean velocity profile. The gradient becomes steeper with increasing H_{12} (see profiles for $\delta_{99} = 0.15 \cdot D$ in Fig.2, right). Figure 8 also reveals that the BLI noise source dominates the RSI source for a sufficiently high shape factor or positive pressure gradient ($H_{12} > 3.00$). Finally Fig.8 reveal that the correct representation of the boundary layer shape by the parameters δ_{99} and H_{12} and the stored TKE is a sensitive parameter in terms of the predicted broadband noise PSD level.

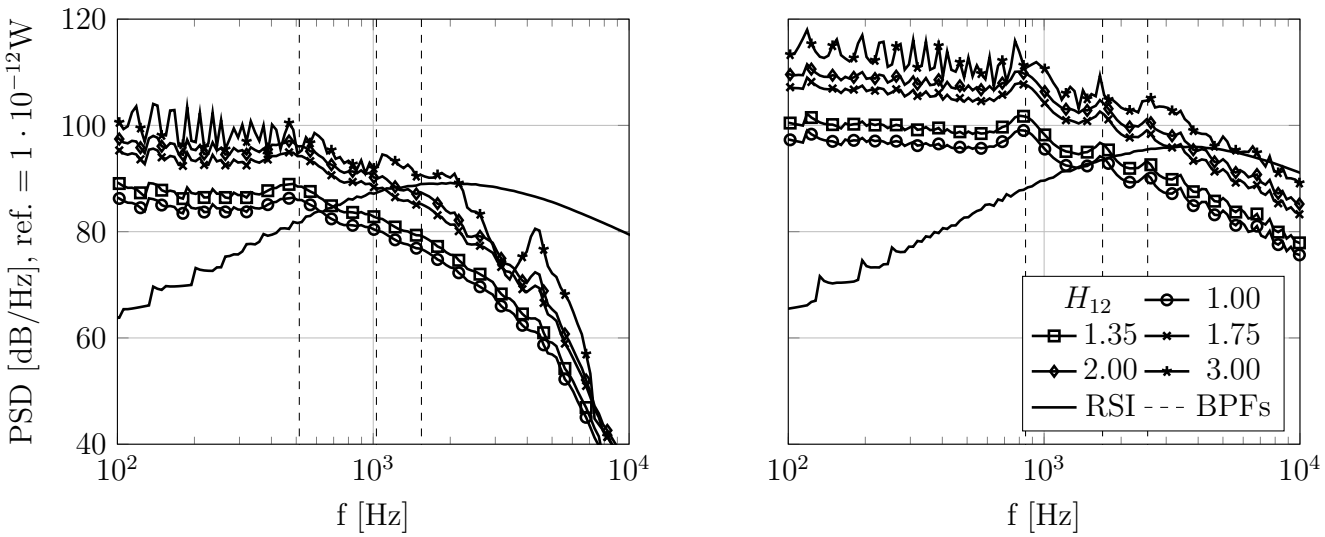

Figure 8: PSD of broadband noise source for Approach (left) and End of Field (right) for different shape factors H_{12} at $\delta_{99} = 0.15\,\mathrm{D}$.

4. Conclusion

A parametric study of a generic turbulent boundary layer interacting with an UHBR fan rotor is presented. The boundary layer model provides the mean flow profile as well as turbulent statistics. Steering parameters are the boundary layer thickness δ_{99} and the shape factor H_{12}, representing the ratio of the displacement thickness to the momentum loss thickness. The latter allows to consider a pressure gradient as it may be expected for a boundary layer entering a turbofan engine. The modeling of the turbulent statistics assumes axially homogeneous and anisotropic turbulence. The impact of both parameters on tonal noise and BBN is investigated. In addition the tonal and broadband rotor-stator wake interaction noise is computed analytically as a reference noise source based on CFD computations.

At zero pressure gradient, an increase of δ_{99} results in a non-simple redistribution of the low-order aerodynamic modes involved in the excitation of the 1$^{\mathrm{st}}$ to 2$^{\mathrm{nd}}$ BPF depending on the operating point. Higher aerodynamic mode orders, exciting the higher BPFs, are slightly reduced. The increase of H_{12} at medium boundary layer thickness increases the modal amplitudes of the lower aerodynamic modes and decreases the amplitudes of the higher ones. Dependent on which aerodynamic modes are involved in the excitation process of cut-on acoustic modes at distinct BPFs, the effect on the PWL is different dependent

on the operating point. Concerning tonal noise the results indicate that RSI remains a significant noise source for AP and EoF.

Concerning broadband noise the increase of δ_{99} or H_{12} is accompanied by an increase of the PWL. The increase of δ_{99} enlarges the region containing turbulence and therefore the overall TKE, generating BBN. The increase of H_{12} magnifies the gradient of the mean velocity profile and therefore the TKE prediction of the used algebraic turbulence model. In addition the study reveals a high sensitivity of the predicted BBN on the correct prediction of boundary layer shape, TKE and integral length scales.

The project leading to this application has received funding from the Clean Sky 2 Joint Undertaking under the European Union's Horizon 2020 research and innovation programme under Grand Agreement No. CS2-GAM-2016-2017-LPA.

REFERENCES

1. Liebeck, R. Design of the Blended Wing Body Subsonic Transport, *Journal of Aircraft*, **41** (1), 10–25, (2004).

2. Moreau, A. *A unified analytical approach for the acoustic conceptual design of fans of modern aero-engines*, Doctoral Thesis, Technical University of Berlin, Germany, (2017).

3. Staggat, M., Moreau, A. and and Guérin, S. Boundary Layer induced Rotor Noise using an Analytical Modal Approach, *Proceedings of the 22nd AIAA/CEAS Aeroacoustic Conference*, Lyon, France, 30 May – 1 June, (2016).

4. Staggat, M., Moreau, A. and and Guérin, S. Improved Analytical Prediction of Boundary-layer induced Rotor Noise using Circumferential Modes, *Proceedings of the International Conference on Fan Noise, Aerodynamics, Applications and Systems (Fan 2018)*, Darmstadt, Germany, 18–20 April, (2018).

5. Kaplan B., Nicke E., Voss C. Design of a Highly Efficient Low-Noise Fan for Ultra-High Bypass Engines, *ASME Paper No. GT2006-90363*, (2006)

6. Coles, D. The law of the wake in the turbulent boundary layer, *Journal of Fluid Mechanics*, **1**, 191–226, (1956).

7. Wilcox, D. C. *Turbulence modeling for CFD*, DCW Industries, La Canada, (1994).

8. Kerschen, E. J., Gliebe, P. R. Noise Caused by the Interaction of a Rotor with Anisotropic Turbulence, *AIAA Journal*, **19** (6), 717–723, (1981).

9. Hunt, J. C. R., Morrison, J. F. Eddy structure in turbulent boundary layers, *European Journal of Mechanics - B/Fluids*, **19**, 673–694, (2000).

10. Haxter, S., Spehr C. Comparison of model predictions for coherence length to in-flight measurements at cruise conditions, *Journal of Sound and Vibration*, **390**, 86–117, (2017).

11. Jaron, R. *Aeroakustische Auslegung von Triebwerksfans mittels multidisziplinärer Optimierungen*, Doctoral Thesis, Technical University of Berlin, Germany, (2018).